Near Surface Geophysics, 2010, **8**, 249-257 doi:10.3997/1873-0604.2010009

Electrical resistivity tomography and induced polarization techniques applied to the identification of gypsum rocks‡

Ander Guinea*, Elisabet Playà, Lluís Rivero and Mahjoub Himi

Department of Geochemistry, Petrology and Geological Prospecting, Faculty of Geology, University of Barcelona, Martí i Franquès s/n, 08028 Barcelona, Spain

Received September 2009, revision accepted April 2010

ABSTRACT

Gypsum deposits are the currently exploited sulphate rocks with industrial purposes. In addition to the expensive drilling projects, geophysical techniques can be considered to estimate the economical potential of these deposits.

An electrical resistivity tomography survey has been carried out in the Pira gypsum formation (SE of the Catalan margin of the Tertiary Ebro Basin, Spain). Additionally, a continuous coring drill was performed in order to support the study. Electrical imaging has been successfully applied to identify the gypsum deposits interlayered in lutite units. Nevertheless, the gypsum-lutite boundaries are diffuse and uncertain in the tomographic lines. Comparison of the cores of the borehole and the electrical response shows a meaningful correlation between electrical resistivity and purity of gypsum. The electrical resistivity tomography profiles display a rather wide range of electrical resistivity value (from 20–1000 Ωm) for the investigated gypsum facies. The highest values are attributed to sulphate layers with >90% of gypsum mineral. Lutite units display higher values than expected due to the presence of evaporite minerals within them (>10 Ωm).

Additionally, induced polarization measures have been performed in order to study the chargeability of gypsum deposits. It has been evidenced that impure gypsum rocks (with important presence of lutites within) are slightly chargeable. This property has allowed distinguishing between lutite levels and clay-rich gypsum rocks.

Electrical resistivity tomography lines are useful in the prospection of gypsum deposits. However, electrical imaging prospection should be supported by an accurate petrological study of the deposits, in order to properly interpret the resistivity profiles.

INTRODUCTION

Evaporites are sedimentary rocks originated from evaporitic processes, this is, have been precipitated from water following the evaporative concentration of dissolved salts. The principal evaporitic mineral groups are sulphates and chlorides. Gypsum is a calcium sulphate with two water molecules ($CaSO_4 \cdot 2H_2O$). It can be found in the nature as primary gypsum (forming selenite crystals or gypsarenite deposits) or as secondary gypsum, coming from the hydration of anhydrite ($CaSO_4$) (displaying alabastrine or megacristalline textures). Principal sulphate rocks (gypsum, anhydrite, glauberite and thenardite) are currently exploited with economical interest (Guinea *et al.* 2009). Gypsum rocks are mainly constituted by gypsum minerals with different amounts of anhydrite, clay minerals and carbonates (calcite and/or dolomite), among others. Evaporitical deposits are characterized by having heterogeneous nature both vertical and horizontally due to primary and secondary processes. Gypsum rocks are impermeable so water cannot run along them. In any case the presence of water can dissolve the deposits creating karst structures.

More than 90 000 tones of industrial gypsum are produced each year in the world. Gypsum is used in the construction sector as primary matter due to its binder property. Furthermore, gypsum is innocuous and has properties of acoustic absorption, thermal insulation and hygrometric regulation. The main gypsum producer countries are USA, Spain, Canada and Iran. To determine the potential economical interest of a gypsum deposit, the aspects to be studied are mainly: a) the thickness of the gypsum layer (a layer has to have at least a width of 1.6 m to be rentable), b) the quantity of clay in the composition of the gypsum rock (it must be less than 20%) and c) the possible structures and discontinuities related to the deposit (due to the possible water filtration that can affect the extractive activity) (Bonetto *et al.* 2008).
Alternative to high cost drilling projects, geoelectrical techniques

‡ This paper is based on the extended abstract P08 presented at the 15th EAGE Near Surface 2009 meeting, 7–9 September 2009 in Dublin, Ireland.

* anderguinea@ub.edu

can be considered to evaluate the exploitability of these deposits (Lugo *et al.* 2008). Electrical resistivity tomography (ERT) is a geophysical technique whose objective is to determine the real electrical resistivity distribution in the subsurface. With this purpose, a DC current is injected in the terrain by two electrodes and the voltage passed through the terrain is measured in two different electrodes along a 2D profile at a certain depth. After processing measured data, a trapeze shaped image displaying the electrical resistivity values is obtained. This image allows us to interpret the distribution of the different materials below the area where the survey took place. The advantages of this method are its non-invasive nature and relative low cost. The measures obtained are indirect and, as occurs in all geophysical techniques, the accuracy of the method decreases with depth. Induced polarization (IP) is an electrical current stimulated phenomenon observed as delayed voltage response in earth materials (the chargeability of the terrain is measured). The fact of measuring different values is enough to define an anomaly (Sumner 1976). Published geoelectrical resistivity values for gypsum oscillate between 10–1200 Ωm (Table 1). Nevertheless, the cause of the wide range of electrical resistivity value of gypsum has not been investigated. These values are higher than the assigned resistivity of lutites (about 1–100 Ωm) (Orellana 1982). The measuring of chargeability in gypsum rocks has not been the object of previous researches but the chargeability properties of clay have been widely studied (Takakura 2006; Deucester and Kaufmann 2009). Nevertheless, the range of chargeability values for clays has not been specifically determined given that many variables are involved (grain size, composition, measure time etc). As a general trend, the clay chargeability values are rather low compared to the chargeability anomalies given by the presence of metallic minerals.

The objective of this study is to characterize the geoelectrical resistivity behaviour of gypsum rocks. It is analysed how the composition of the rocks (purity in gypsum mineral and the presence and nature of the accompanying minerals) affects the electrical resistivity value. Moreover, the chargeability of this material is discussed in order to obtain additional information that allows us to characterize the deposits. The survey is carried out

TABLE 1
Published electrical resistivity values for gypsum rocks

Reference	Resistivity value (Ωm)	Author's comments
Lugo *et al.* (2008)	80–100	The lower values are related to the presence of lutites within the gypsum rocks. The higher values correspond to the presence of anhydrite within gypsum.
Ball *et al.* (2006)	25–500/500–1000	The values are directly obtained from inverted geoelectrical profiles. There are two ranges of values depending on the porosity of gypsum.
Asfahani and Mohammad (2002)	24–1200	The values are measured by vertical electrical soundings in the gypsum and anhydrite formation.
Benson and Kaufmann (2001)	100–150/>300	The lower range is considered for unconsolidated gypsum sediments. Unweathered gypsum has a value greater than 300 Ωm.
Rider (1986)	1000	The values are obtained from measuring electrical resistivity by a diagraphy system.
Orellana (1982)	10–1000	The lower values are related to marls. When gypsum is associated with anhydrite, the electrical resistivity value can overcome 1000 Ωm.

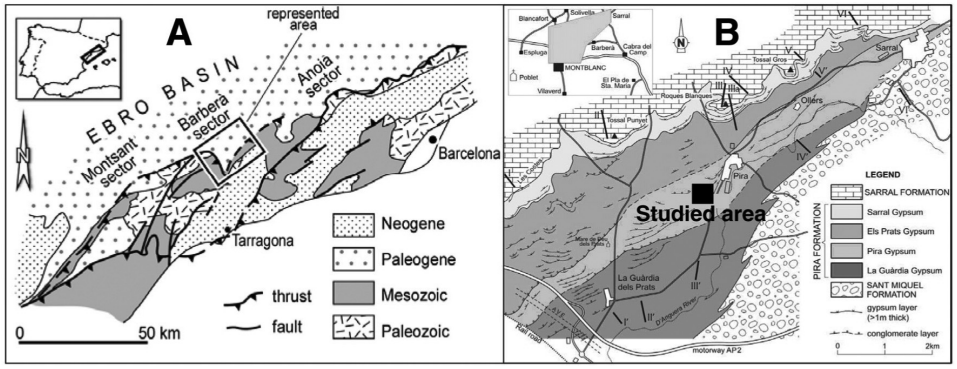

FIGURE 1
a) Geological location of the Barberà sector in the SE margin of the Ebro Basin (NE Spain).
b) Geological map of the Eocene evaporite units composing the Pira Fm (modified from Ortí *et al.* 2007). The black square indicates the studied area.

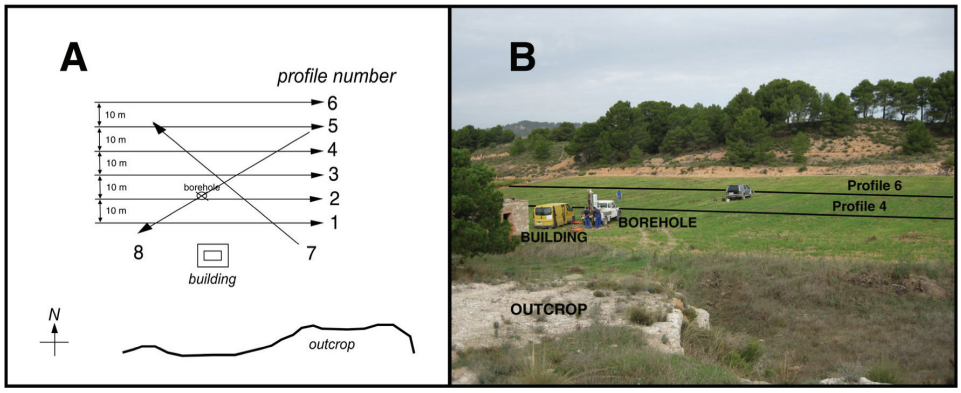

FIGURE 2
a) Sketch and b) photograph of the performed imaging profiles (1–8) and location of the Pira borehole in the studied plot (Pira Village, Tarragona, NE Spain). General location of the studied plot of land in Fig. 1.

by indirect (electrical techniques) and direct methods (borehole) in order to compare them.

MATERIALS AND METHODS

Eight ERT profiles were performed in the studied gypsum formation (Fig. 1), located close to the Pira village (Tarragona, NE Spain). The disposition of the profiles was parallel and E–W orientated, with the exception of two oblique profiles.

There are lots of different arrays used in the electrical prospection methods (Szalai and Szarka 2008) with a different depth of investigation and vertical resolution values (Szalai *et al.* 2009). In this survey some of the most used arrays for ERT were tried (dipole-dipole, Wenner alpha and Wenner-Schlumberger) showing similar results. Finally Wenner-Schlumberger was selected given that the unit dips less than 15º NNW and displays apparent lateral continuity. The measures of apparent electrical resistivities were made with a SYSCAL PRO switch with 48 electrodes separated by 2 m between them with internal power supply. In three of these ERT profiles, IP in time-domain measures were acquired with arithmetic configuration for a 500 ms time lapse (Dahlin *et al.* 2002). With the purpose of processing data, the RES2DINV program was used to carry out the inversion. This program uses the smoothness-constrained least-squares method (deGroot-Hedlin and Constable 1990; Sasaki 1992) in its inversion routine.

An additional 15 m continuous coring drill was done in the plot to support the imaging prospection campaign (Fig. 2). The cores were accurately petrographically described and sampled. The amount of non-gypsum minerals was quantified by the dissolving of about 0.5 g of 6 powdered gypsum samples in 250 mL of distilled water (solubility of gypsum is about 2.4 g/L); solutions were shook during 24 hours and subsequently filtered. The remnant after filtering corresponds to the non-soluble impurities of the gypsum rock. The results of these laboratory essays are not absolutely representative of the whole deposit due to the lixiviation of finest materials (lutites) during the water-mediated drilling works. The residual material was mineralogically characterized by X-ray diffraction (XDR). In addition, representative thin sections of the whole deposit have been studied under a standard petrographic microscope.

GEOLOGICAL SETTING

During the Paleogene, an evaporitic lacustrine sedimentation episode took place along the SE of the Catalan margin of the Tertiary Ebro Basin (Ortí 1990a,b ; Ortí *et al.* 2007). The Conca de Barberà sector (where the study is situated) is a depression excavated on the Eocene and Oligocene materials of the Ebro basin (Fig. 1a). In the Catalan margin the sedimentation was bound to the tectonic evolution of the Catalan Coastal Range. During the Paleogene compression NNW verging structures, as folds and thrusts, developed in the area. These structures were related to pre-existing basement faults. In the Miocene, these structures acted as normal faults during an extensional episode (Anadón *et al.* 1985; Cabrera *et al.* 2004).

The studied materials correspond to the Pira Gypsum of the Pira member, belonging to the Montblanc formation. They are characterized by secondary gypsum in the surface (coming from hydration of anhydrite) and anhydrite at depth. At some levels, the gypsum appears in centimetric nodules (sometimes up to metric sized nodules) or enterolithic layers. These structures are inherited from anhydrite (Ortí *et al.* 2009). Several gypsum units, with individual thicknesses ranging from 50–100 m, are intercalated within various detritic units.

The studied units can be separated into two different terms. The lower term is constituted of red lutites with few intercalations of sandstones. The upper term is less terrigenous than the lower one and corresponds to the evaporite sequence. Additionally, there are lateral variations in the composition of gypsum deposits related to depositional processes. Depending on the position of the gypsum precipitation within the lacustrine basin, the quantity of lutite in the gypsum rock is low (offshore) or high (near the shore). This is due to the proximity of terrigen contribution.

The plot of land where the profiles and the well were performed is located near the Pira village (Fig. 1b). The outcropping gypsum layers (at the southern part of the terrain) are expected to be represented in the ERT image.

RESULTS

A total of 8 electrical resistivity profiles were carried out in the studied area. In the performed ERT profiles the root-mean-square (rms) error between the measured and calculated values

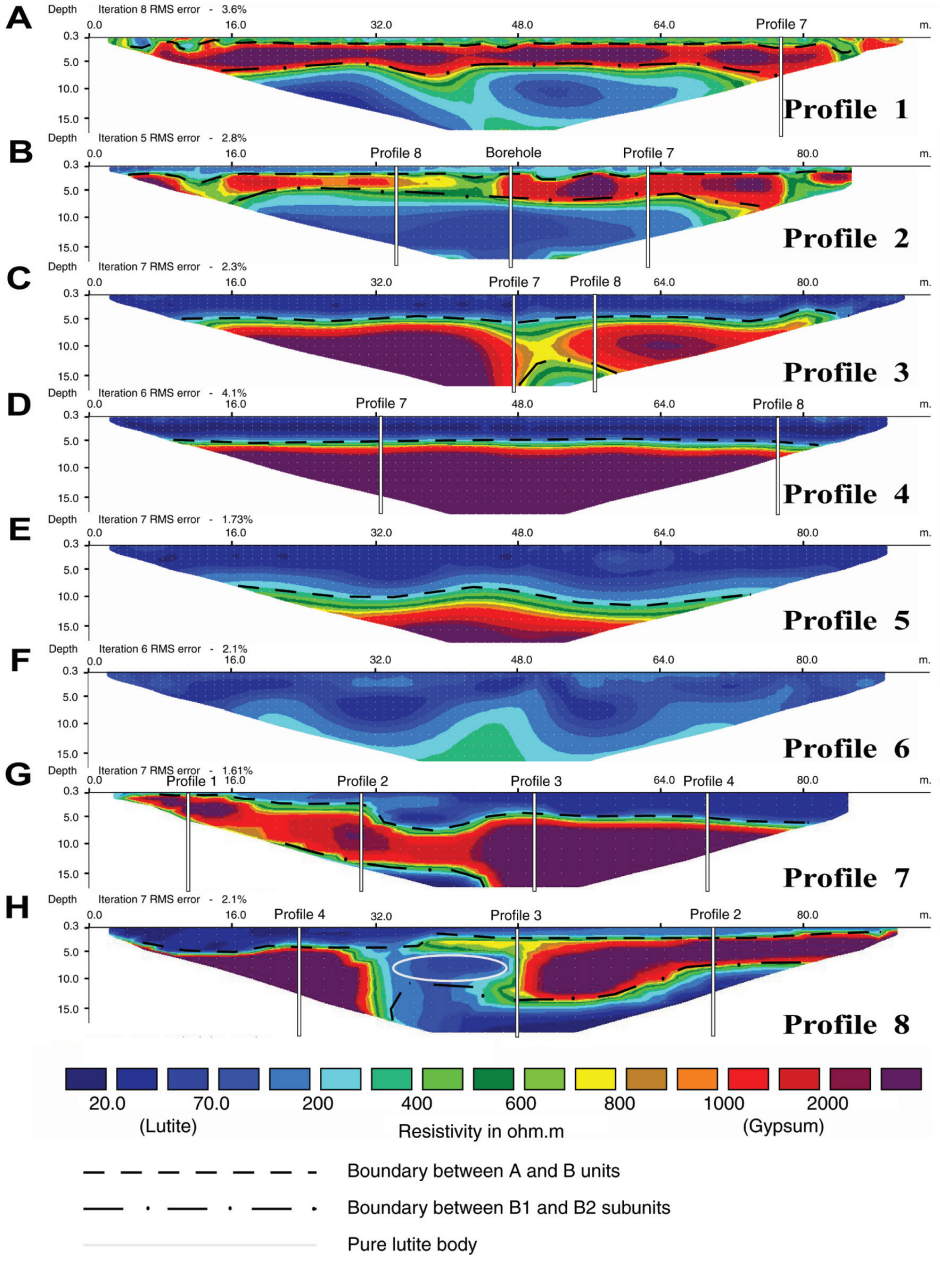

FIGURE 3
Electrical imaging profiles (Pira village, Ebro Basin, NE Spain). Location of the profiles in Figs 1 and 2. The profiles show the points where they are cut by other profiles and the situation of the borehole.

was low (<5%). Two types of materials are observed in all the images: a) materials with low electrical resistivity values (1–50 Ωm), blue in colour and b) materials with high electrical resistivity values (>900 Ωm), displaying red-purple colours (Fig. 3). The intermediate values are assigned to the transition between these two types of materials, which depend in turn on the depth. Given that the resolution decreases with depth, these boundaries are well defined in the ERT lines when they are shallow and diffuse when they are at the lower part of the profile (as in Fig. 3e).

The real electrical resistivity profiles 1 and 2 (Fig. 3a,b) show a surface layer (up to 1–2 m depth) composed of low electrical resistivity materials (~10 Ωm); this level is overlaying a high electrical resistivity material body (80–1000 Ωm). Underneath this resistive body, resistivity decreasing materials are recorded from a depth of 7 m (~800 Ωm) to 12 ms (<100 Ωm). In profiles 4 and 5 (Fig. 3d,e), the resistive body is thicker and continues at depth. The deeper low electrical resistivity materials do not appear in these profiles. The boundary between the superficial layer and the resistive body is slightly tilted towards north, as clearly reflected in profiles 7 and 8 (Fig. 3g,h), thus making thicker the uppermost low resistive body from profile 1–6. In profile number 6 (Fig. 3f), which is the northern one, this boundary is not cut by the ERT. In order to get a better view of the deposit, a 3D resistivity model of the studied area has been carried out by interpolation of the inverted resistivity data. This

model is displayed as horizontal slices at different depths in Fig. 4. A trend of high resistivity values moving towards north can be seen, while the depth increases.

The chargeability of the terrain was measured in profiles 2, 7 and 8. The IP anomalies (until 6 mV/V) have a trend in accordance with the resistivity decreasing materials in the ERT profiles (Figs 5a–c and 6), indicating a lithologic control. The match between the trend of IP values and the lithologic composition is especially good in the case of profile 2, which is parallel to the stratification. In the case of profiles 7 and 8, which are oblique to the structure, the boundary between gypsum impure layers and the lutite layers is undefined in the IP imaging. All the profiles show a surface layer with background values (1.5–2.5 mV/V), which match with the low electrical resistivity surface values from unit A (Fig. 6) and a depth-increasing anomaly, up to 6 mV/V. In profile 2 this anomaly decreases below 12 m.

A detailed petrological study of the Pira cores from the Pira well has permitted to distinguish several subunits in the gypsum layer, according to the gypsum lithofacies and the amount of accompanying minerals. The studied gypsum layer is mainly constituded of microcrystalline massive gypsum (with traces of anhydrite within) with diffuse bedding and lamination (Fig. 7). Nodules of microcrystalline (alabastrine) pure gypsum and chert and patches of carbonates are frequent. Reddish and brownish colours in gypsum are due to the irregular presence of enclosing clays and carbonates (calcite and dolomite) within the gypsum matrix, respectively. The purity of the gypsum rock is from 56.3–93.9% (Fig. 6) and colouring from white to red-brown is

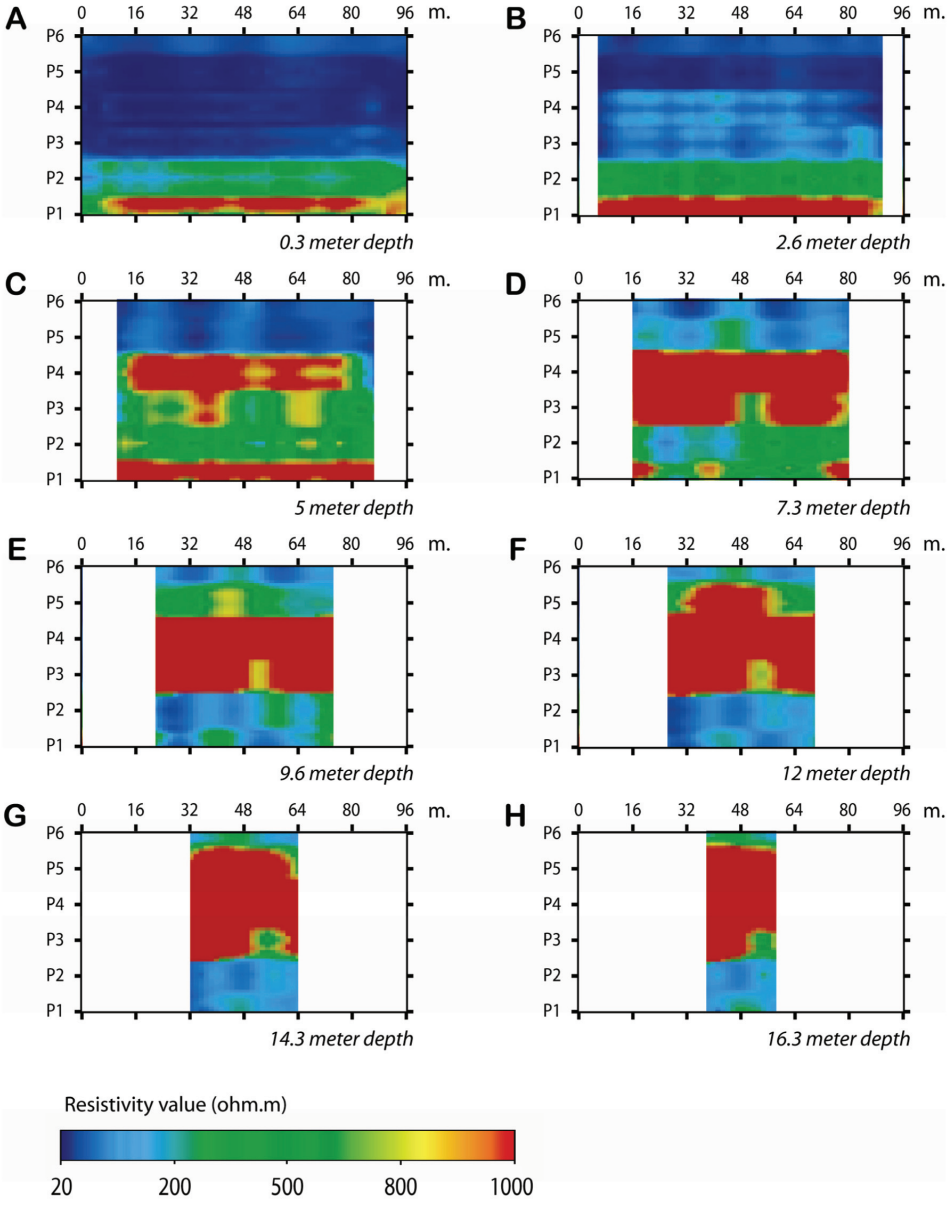

FIGURE 4
Horizontal slices at a different depth of the studied area showing the electrical resistivity values. The slices have been elaborated from the interpolation of the ERT profiles in Fig. 3. The location of the profiles is marked with P and its corresponding number in the Y-axis of each slice.

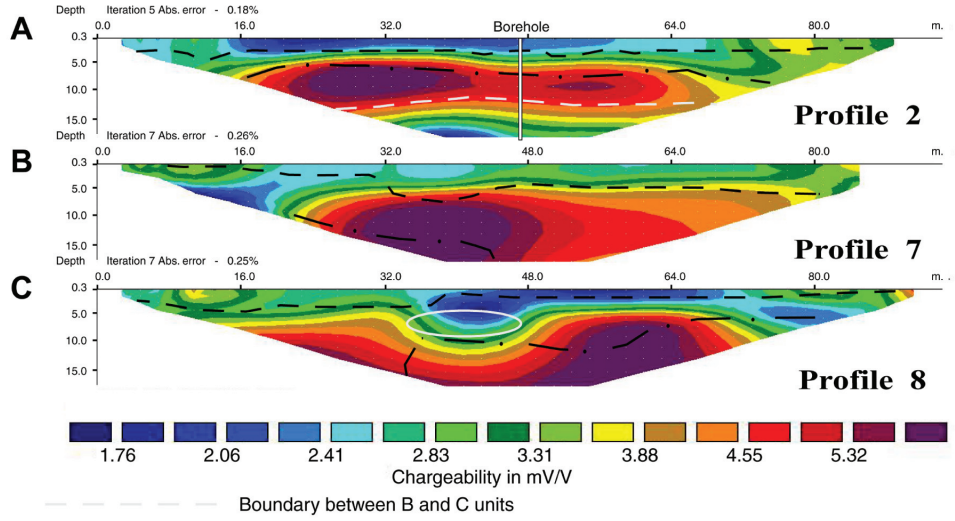

FIGURE 5
Electrical chargeability profiles (Pira village, Ebro Basin, NE Spain). Location of the profiles in Figs 1 and 2. The B-C boundary is interpreted from IP measuring.

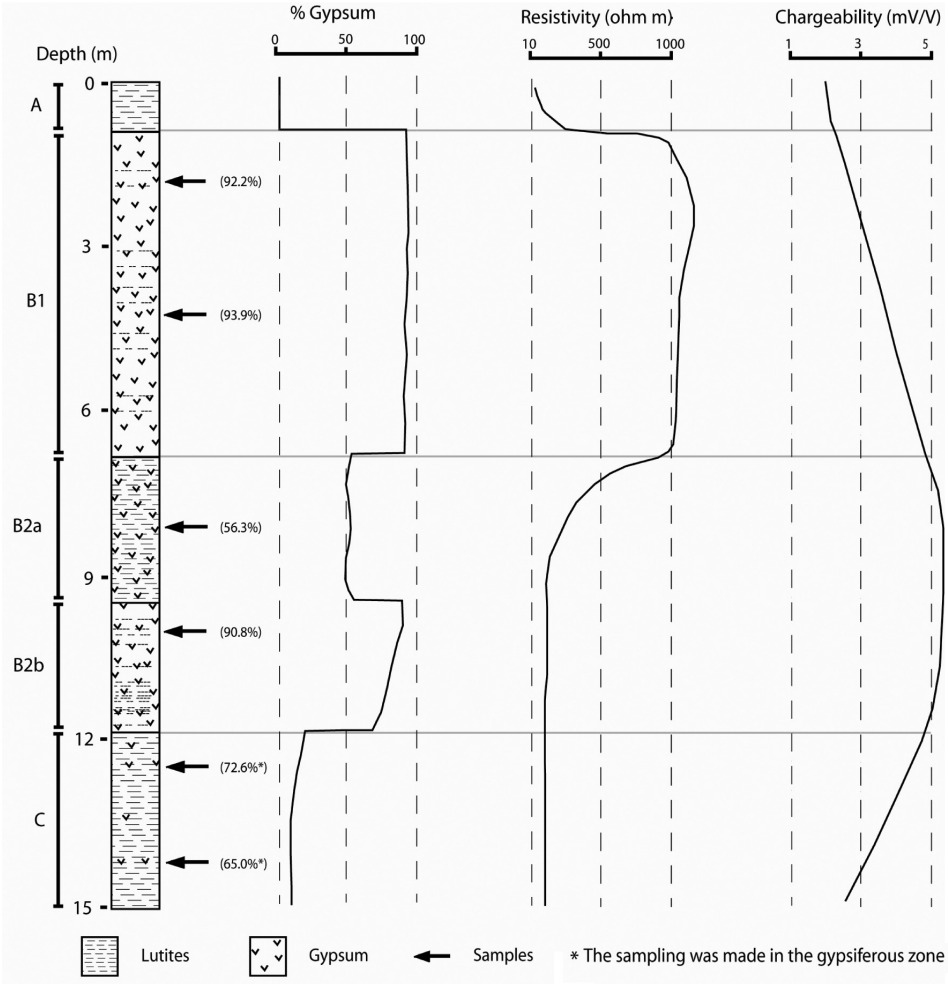

FIGURE 6
Simplified log of the Pira well (Ebro Basin) and relationships between the purity of the gypsum rocks and their geoelectrical response. Values in brackets indicate the percentage of gypsum in the analysed samples. The % gypsum curve is extrapolated from the sampling; the resistivity and the chargeability curves are taken from the values displayed in profile 2 from Figs 3(b) and 5(a).

directly related to the increase of enclosing minerals. The residue from the essays (formed by the non-evaporitic phases) is constituted by clay minerals, carbonates (calcite and dolomite), quartz and celestite. Regarding the percentages obtained in the purity analyse, it must be noted that the drilling process was water-mediated, which solved the little quantity of gypsum at the first metres of the drilling (the fluid that left from the borehole was white in colour). The cores recovered below a depth of 6.8 m were smaller and fractured and the water used in the perforation became brownish (because of clay leaching). This suggests that

an important amount of clay minerals was leached and therefore the real purity of gypsum would be even lower than measured in the analysis.

DISCUSSION

The target of the study is a gypsum layer, overlayed by lutites, which was exploited in the XX century. The five uppermost metres of the unit outcrop in the walls of the old quarries. Three different units have been described in the imaging profiles. They are interpreted as (from top to bottom): a) a lutite surface soil, b) a gypsum layer and c) a basal lutite unit, which is only present in profiles 1 and 2 (Fig. 3a,b). The real resistivity sections display a disposition sinking toward to the north; this dipping can be measured at the southern outcrop.

The uppermost gypsum-lutite boundary is well-defined in the tomographyc profiles, due to the high resistivity contrast between lutites and gypsum (around 10 Ωm for the lutites and higher than 800 Ωm for the gypsum rocks). The calculated values for gypsum at some ERT profiles (>2000 Ωm) are higher than the values given in Table 1. This is due to the difficulties of the electric current to pass through the resistive levels; on these gypsum levels the sensitivity of the method in data acquisition decreases, giving anomalous values. Nevertheless, even the values are not totally realistic, the general structure is well-defined. The electrical resistivity slices show that the boundaries are neat and E–W oriented (Fig. 4). The slices display the layer of the evaporitical deposit sinking towards north at depth represented by the high resistivity values.

In the log-description, the gypsum unit is divided into (Fig. 6): 1) upper B1 subunit, from 0.9–6.8 m depth, made of pure (purity up to 94%), massive and white to brownish secondary microcrystalline gypsum and 2) lower B2 subunit, from 6.8–11.8 m depth, formed by massive to laminated reddish secondary microcrystalline gypsum with abundant red lutites (purity of gypsum from 56–91%). The B2 subunit can be separated into 2 additional terms in relation to its composition: a) where the composition is very lutitic (around 50%) and b), whose purity decreased with depth starting from a pure composition (around 90%). The samples from the outcrop, whose purity has been analysed, would correspond to the first 5 m of the B1 subunit. The purity obtained in these samples (99% and 91%) matches with the purity obtained on core samples at those depths (92.2% and 93.9%). The change of composition in the gypsum rocks has a sedimentary origin. Lateral variations (in composition and thickness) are current in evaporite rocks. The evaporite deposits can be very heterogeneous because its precipitation is usually bonded to an irregular input of detritical particles.

The comparison of the composition (% of gypsum) of the samples from the cores with the resistivity values obtained in profile 2 (Fig. 6) evidences that the uppermost lutite-gypsum boundary is abrupt and well-defined. The resistivity values of lutites are lower than 20 Ωm and values of 800 Ωm are rapidly achieved at 0.9 m depth. This boundary surface (boundary between A and B units) is clearly recorded in profiles 1–8, whose depth at each profile is in accordance with the NNW dipping of the layers. Conversely, the lowermost gypsum-lutite boundary (boundary between B and C units) is progressive and diffuse in tomographyc profiles 1 and 2; the resistivity values decrease from 800 Ωm, at 6.8 m depth (which represents the boundary between B1 and B2 subunits), to 100 Ωm, at 12 m depth. Thus, geological interpretation of the ERT profiles could be confusing and uncertain, while the boundary between B and C units is clearly recognized at 11.8 m depth in the Pira well. With the information obtained from the core is evidenced that the progressive decreasing of resistivity in 1 and 2 ERT profiles is due to B2 subunit presence. This phenomenon is related to a decreasing of gypsum purity in the whole-rock. However, it is not possible to distinguish between B2a and B2b terms in the ERT lines because of the resolution of the method (Sumanovac and Dominkovic 2007). The value of electrical resistivity becomes stable at 12 metres depth, with a value of 20 Ωm; this reflects the boundary between B and C units. The C unit contains a minor quantity of dispersed gypsum, which slightly increases the value of resistivity with respect to those of the lutites (<10 Ωm).

The highest resistivity values in profile 2 correspond to the purest gypsum level (B1 subunit). Conversely, the highest chargeability values are registered in the B2 subunit, which is richer in lutites than the previous one. Additionally, the boundary between B and C units (found at 12 m in the borehole), which is not shown at the electrical imaging, matches with the chargeability decreasing in profile 2. This boundary is interpreted in Fig. 7(a). The increasing of the chargeability values can be explained as an electrical condenser effect produced by the alternation of thin clay laminae and gypsum thin laminae, where gypsum would act as a dielectric material. There is another possible explanation based on the dispersion and absorption of electrical currents in dielectric materials. Cole and Cole (1941) defined the parameters for molecular scale polarization interactions in scattered ions. On a macroscopic scale, the Cole-Cole parameters have been resolved from chargeability values given by metallic mineral particles in a rather poorly conducting matrix (Efferso 2006).

The most plausible lithological interpretation of the studied area is displayed in Fig. 8, on the basis of the geoelectrical response of the materials (both resistivity and chargeability) and the stratigraphical and petrological studies. This model corresponds to the evaporitical structure in the situation of profile 8, which is representative of the whole evaporitic deposit. All the boundaries between the units are sedimentary in origin, showing common lateral and vertical compositional changes. The horizontal variation of purity between B1 and B2 unities is interpreted as a transition. Towards north, the thickness of the gypsum body increases. The centre of the evaporitical basin would be in the same direction. However, the southern part would receive the influence of terrigen contribution, which is represented by the B2 unit. The electrical resistivity imaging has allowed defining the body of pure gypsum and its change of purity. In profile 8 is also displayed a lutite body

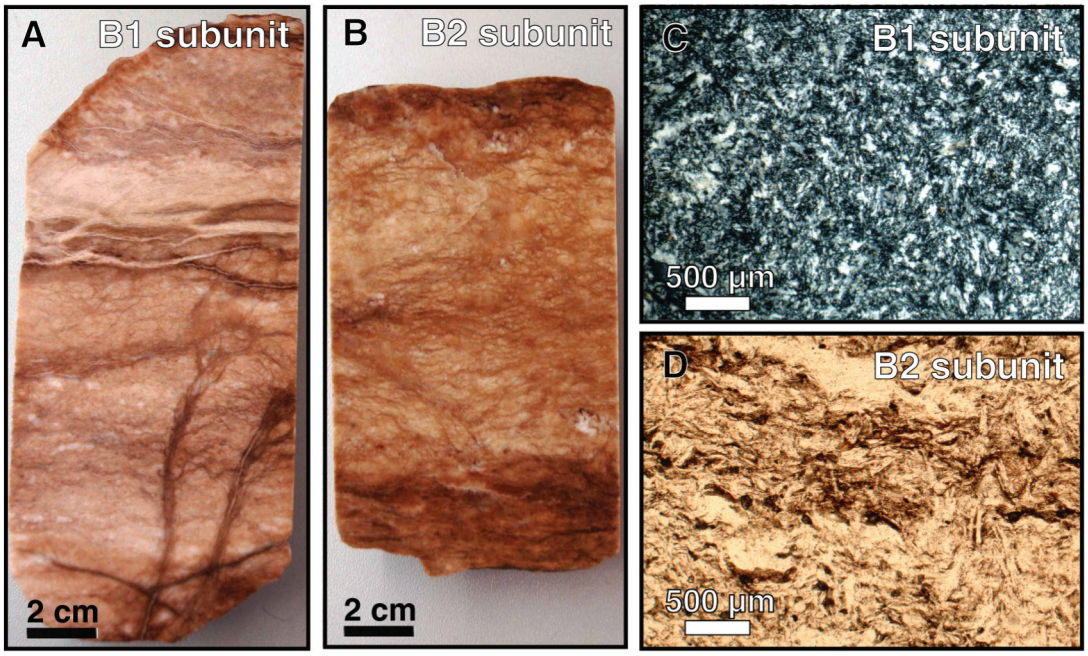

FIGURE 7

a) Hand sample of the Pira core from the B1 subunit. Even with the brownish colouring of the core, which is due to the disperse presence of calcite, the main constituent is gypsum (>90%). b) Hand sample of the Pira core from the B2b subunit. The reddish colouring is due to the presence of clay-rich laminae. c) Photomicrograph (cross polarized light) of the gypsum rock from the B1 subunit with alabastrine texture (microcrystalline pure gypsum). d) Photomicrograph (plane polarized light) of the non-pure gypsum rock from the B2a subunit, showing diffuse clay-rich laminae within the host-gypsum rock. Pseudomorphs of anhydrite crystals (prisms), replaced by gypsum, are evidenced.

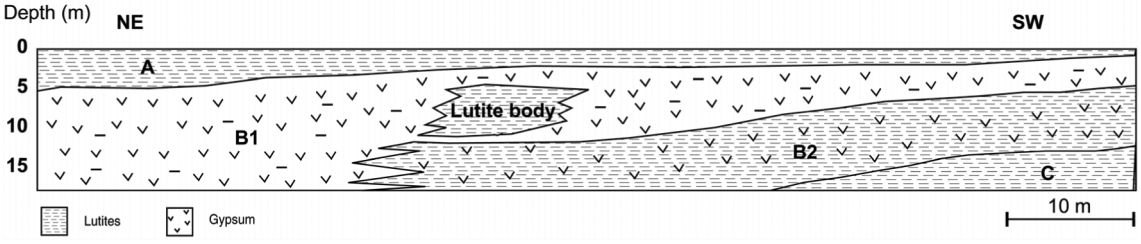

FIGURE 8

Interpretative model based on the ERT and IP images from profile 8 (location in Fig. 2). The different units A, B and C of the log (defined in Fig. 6) are displayed together with the lutite body.

without gypsum within. This body would be explained as a local small mound when deposition took place. Another possible explanation is synsedimentary dissolution, created by a water current channel with following lutite infilling. There is no evidence of large dissolution in this area but there is also the possibility of recent local-scale dissolution. The body is located in a less resistive area that is related to the presence of more lutite; this is shown in the centre part of the slice at 5 m depth (Fig. 4c).

The fact of having a 3D structure could have affected the measurements (Nyári and Kamli 2007) but in this case the lateral changes are not abrupt and the ERT profile images are coherent between them (profiles 1–6 respect 7 and 8, which are oblique). In the case of chargeability measurement, it has permitted to interpret the lutite inclusion in addition to distinguish between impure gypsum and pure lutite.

CONCLUSIONS

1 A laboratory test was employed to measure the percentage of insoluble residue in gypsum core samples. The purity of analysed gypsum rocks is from 56–64% of gypsum mineral. Accompanying minerals (insoluble residue) are clay minerals, calcite and dolomite, quartz and celestite.

2 a) Electric imaging has been successfully applied to identify the gypsum deposits interlayered in lutite units. Nevertheless, the gypsum-lutite boundaries can be shown as diffuse and uncertain in the tomographic lines (mainly at depth).

b) A meaningful correlation between electric resistivity and purity of gypsum rocks has been determined. It is clear that resistivity for the investigated gypsum facies varies in a rather wide range, from 20–1000 Ωm.

c) Three sets of resistivity data have been obtained: the lutite layers, the purest gypsum rocks and the non-pure gypsum units have resistivity values up to 20 Ωm, between 700–1000 Ωm and from 20–700 Ωm, respectively.

3 a) It is possible to distinguish between pure lutites, pure gypsum and clay-rich gypsum layers (if they are within pure gypsum layers) by means of the chargeability values. In non-pure gypsum rocks, the gypsum minerals can act as a dielectric material giving an electrical condensation phenomenon in the clay particles within.

b) Resistivity and chargeability measures permit to distinguish between lutite levels and clay-rich gypsum rocks, with similar low electrical resistivity values to lutites.

4 Boreholes are very useful as supporting the interpretation due to the petrological complexity of evaporitic formations.

The obtained results show that electrical resistivity lines could be useful in the mapping and prospection of gypsum deposits. However, imaging prospection should be supported by an accurate petrological study of the deposits (distinguishing between pure and non-pure gypsum rocks), in order to properly interpret the resistivity images.

ACKNOWLEDGEMENTS

The present work was supported by the 'Programa General de Intensificació de la Investigació' (Generalitat de Catalunya-UB) and the Spanish Government Projects CGL2009-11096, CGL2009-07025 and CGL2006-04860. We appreciate the support and facilities of Dr A. Casas and Dr J. Esteve (University of Barcelona, Spain). We also thank the reviewers for their comments, which have helped us to improve the manuscript.

REFERENCES

Anadón P., Cabrera L., Guimerà J. and Santanach P. 1985. Paleogene strike-slip deformation and sedimentation along the southeastern margin of the Ebro Basin. In: *Strike-slip Deformation, Basin Formation and Sedimentation* (eds K. Biddle and N. Christie-Blick), pp. 303–318. Society of Economic Palaeontologists and Mineralogists.

Asfahani J. and Mohamad R. 2002. Geo-electrical investigation for sulphur prospecting in Teshreen Structure in Northeast Syria. *Exploration and Mining Geology* **11**, 49–59.

Ball L.B., Lucius J.E., Land L.A. and Teeple A.P. 2006. Geological Survey Scientific Investigations Report 2006. US Geological Survey.

Benson R.C. and Kaufmann R.D. 2001. Characterization of a highway sinkhole within the gypsum karst of Michigan. In: *Geotechnical and Environmental Applications of Karst Geology and Hydrology* (eds B.F. Beck and J.G. Herring), pp. 103–112. Taylor & Francis.

Bonetto S., Fornaro M., Giulani A. and Lasagna M. 2008. Underground quarrying and water control: Some cases from Nothern Italy. 10th International Mine Water Association Congress, 2008, Czech Republic, Expanded Abstracts, P02.

Cabrera Ll., Roca E., Garcés M. and de Porta J. 2004. Estratigrafía y evolución tectonosedimentaria oligocena superiorneógena del sector central del margen catalán (Cadena Costero- Catalana). In: *Geologia de España* (ed. J.A. Vera), pp. 569–573. Sociedad Geológica de España-Instituto Geológico y Minero de España, Madrid (in Spanish).

Cole K.S. and Cole R.H. 1941. Dispersion and absorption in dielectrics. *Journal of Chemical Physics* **9**, 341–351.

Dahlin T., Leroux V. and Nissen J. 2002. Measuring techniques in induced polarisation imaging. *Journal of Applied Geophysics* **50**, 279–298.

Deucester J. and Kaufmann O. 2009. Correlation between inverted chargeabilities and organic compounds concentrations in soils-A field experiment. 15th Near Surface meeting, Dublin, Ireland, Expanded Abstracts, C19.

Efferso F. 2006. Resolution of Cole-Cole parameters based on induced polarization data. In: *Methods and Applications of Inversion* (eds P.C. Hansen, B.H. Jacobsen and K. Mosegaard), pp. 120–128. Springer.

deGroot-Hedlin C. and Constable S. 1990. Occam's inversion to generate smooth, two-dimensional models from magnetotelluric data. *Geophysics* **55**, 1613–1624.

Guinea A., Playà E., Rivero L. and Himi M. 2009. Importance of gypsum purity in electric imaging. 15th Near Surface meeting, Dublin, Ireland, Expanded Abstracts, P08.

Lugo E., Playà E. and Rivero Ll. 2008. Aplicación de la tomografía eléctrica a la prospección de formaciones evaporíticas. *Geogaceta* **44**, 223–226 (in Spanish).

Nyári Z. and Kanlı A.I. 2007. Imaging of buried 3D objects by using electrical profiling methods with GPR and 3D geoelectrical measurements. *Journal of Geophysics and Engineering* **4**, 83–93.

Orellana E. 1982. *Prospección geoeléctrica en corriente continua*. Paraninfo.

Ortí F. 1990a. Introducción a las evaporitas de la Cuenca Terciaria del Ebro. In: *Formaciones evaporíticas de la Cuenca del Ebro y cadenas periféricas, y de la zona de Levante* (eds F. Ortí and J.M. Salvany), pp. 62–66. Universidad de Barcelona-Enresa.

Ortí F. 1990b. Las formaciones evaporíticas del Terciario continental de la zona de contacto entre la Cuenca del Ebro y los Catalánides. In: *Formaciones evaporíticas de la Cuenca del Ebro y cadenas periféricas, y de la zona de Levante* (eds F. Ortí and J.M. Salvany), pp. 70–75. Universidad de Barcelona-Enresa.

Ortí F., Rosell L. and Playà E. 2007. Depositional models of lacustrine evaporites in the SE margin of the Ebro Basin (Paleogene, NE Spain). *Geologica Acta* **5**, 19–34.

Ortí F., Rosell L. and Playà E. 2009. Meganodular anhidritisation: a shallow to moderate burial mechanism of gypsum-to-anhydrite conversion. *Geological Quarterly* (submitted).

Rider M.H. 1986. *The Geological Interpretation of Well Logs*. Blackie Halsted Press.

Sasaki Y. 1992. Resolution of resistivity tomography inferred from numerical simulation. *Geophysical Prospecting* **40**, 453–463.

Sumanovac F. and Dominkovic S. 2007. Determination of resolution limits of electrical tomography on the block model in a homogenous environment by means of electrical modelling. *Rudarsko Geolosko Naftni Zbornik* **19**, 47–56.

Sumner J.S. 1976. *Principles of Induced Polarization for Geophysical Exploration*. Elsevier.

Szalai S., Novák A. and Szarka L. 2009. Depth of investigation and vertical resolution of surface geoelectric arrays. *Journal of Environmental & Engineering Geophysics* **14**, 15–23.

Szalai S. and Szarka L. 2008. On the classification of surface geoelectric arrays. *Geophysical Prospecting* **56**, 159–175.

Takakura S. and Nakada K. 2006. IP measurements on tunnel walls of a sericite deposit – A contact method of nonpolarizable electrodes on a base rock and detection of clay minerals by normalised chargeability. *Geophysical Exploration* **59**, 363–370.